

A Plug-and-Play Learning-based IMU Bias Factor for Robust Visual-Inertial Odometry

Yang Yi, Kunqing Wang, Jinpu Zhang, Zhen Tan, Xiangke Wang, Hui Shen* and Dewen Hu*

Abstract—The bias of low-cost Inertial Measurement Units (IMU) is a critical factor affecting the performance of Visual-Inertial Odometry (VIO). In particular, when visual tracking encounters errors, the optimized bias results may deviate significantly from the true values, adversely impacting the system’s stability and localization precision. In this paper, we propose a novel plug-and-play framework featuring the Inertial Prior Network (IPNet), which is designed to accurately estimate IMU bias. Recognizing the substantial impact of initial bias errors in low-cost inertial devices on system performance, our network directly leverages raw IMU data to estimate the mean bias, eliminating the dependency on historical estimates in traditional recursive predictions and effectively preventing error propagation. Furthermore, we introduce an iterative approach to calculate the mean value of the bias for network training, addressing the lack of bias labels in many visual-inertial datasets. The framework is evaluated on two public datasets and one self-collected dataset. Extensive experiments demonstrate that our method significantly enhances both localization precision and robustness, with the ATE-RMSE metric improving on average by 46%. The source code and video will be available at <https://github.com/yiyiscut/VIO-IPNet.git>.

I. INTRODUCTION

In recent years, high-precision and robust localization technologies have become critical in industrial applications, particularly in robotics [1], [2] and augmented reality [3]. As the cost and size of vision sensors and Inertial Measurement Units (IMU) continue to decline, their adoption has become increasingly widespread. The complementary nature of vision sensors and IMU in data measurement has further propelled their integration, establishing Visual-Inertial Odometry (VIO) as a key method for achieving advanced localization capabilities.

The IMU provides high-frequency angular velocity and acceleration data that effectively compensate for tracking errors in vision-only systems. However, the measurements are prone to drift due to factors such as temperature, a challenge particularly pronounced in low-cost devices. This drift is typically modeled as the combination of bias error and random error. When visual feature quality is high, visual data predominates, and the estimator leverages the constraints between visual and inertial data to estimate the bias [4]. Conversely, when visual features are compromised, optimization-based VIO frameworks often lack robust constraints on IMU

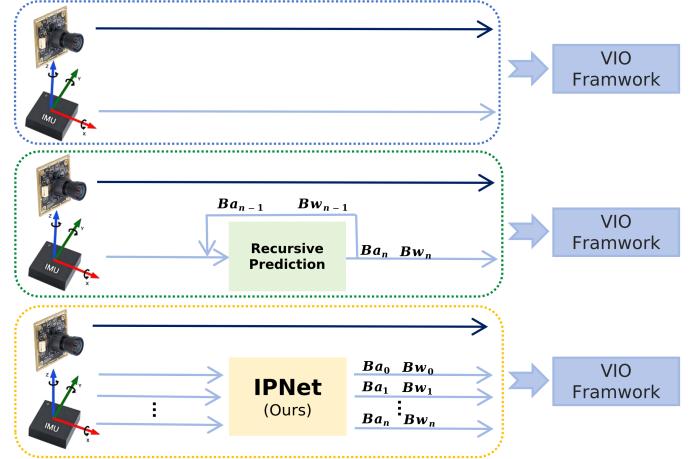


Fig. 1. Comparison of IPNet with recursive prediction methods for IMU bias estimation. IPNet directly estimates bias from raw IMU data, preventing error propagation, while recursive methods rely on historical estimates. The prior factors constructed by it significantly enhance both localization precision and robustness.

bias estimation, leading to significant deviations between the estimated and actual bias values over certain time intervals. These issues undermine the precision and robustness of localization systems, limiting their effectiveness in demanding scenarios.

Existing methods for IMU bias estimation in optimization-based VIO frameworks face significant limitations. For instance, the baseline approach using monocular and inertial data in VINS-Fusion [5] struggles with unfounded adjustments of the bias during optimization, often forcing the bias to fit visual constraints inaccurately. In recent years, researchers have attempted to address this issue using deep learning methods, as seen in [6], by modeling the dynamic evolution of IMU bias. However, the proposed method heavily rely on the estimation results from the previous time step, leading to continuous error propagation once a mistake occurs. This problem is particularly pronounced when the initial values are inaccurate, and it can even lead to trajectory divergence. To overcome these limitations, we propose the Inertial Prior Network (IPNet), which directly estimates IMU bias in real time from raw IMU data, eliminating the dependency on historical estimates in traditional recursive predictions. Furthermore, considering the difficulty of obtaining real-time, accurate IMU bias labels during motion, we use the average bias of each sequence as the label. This approach simplifies the training process while maintaining accuracy. Finally, recognizing that many visual-

Y. Yi, K. Wang, J. Zhang, Z. Tan, X. Wang, H. Shen and D. Hu are with the College of Intelligence Science and Technology, National University of Defense Technology, China.

* indicates corresponding authors: H. Shen(shenhui@nudt.edu.cn) and D. Hu(dwuh@nudt.edu.cn)

This work was supported in part by the Science and Technology Innovation Program of Hunan Province (2024QK2006).

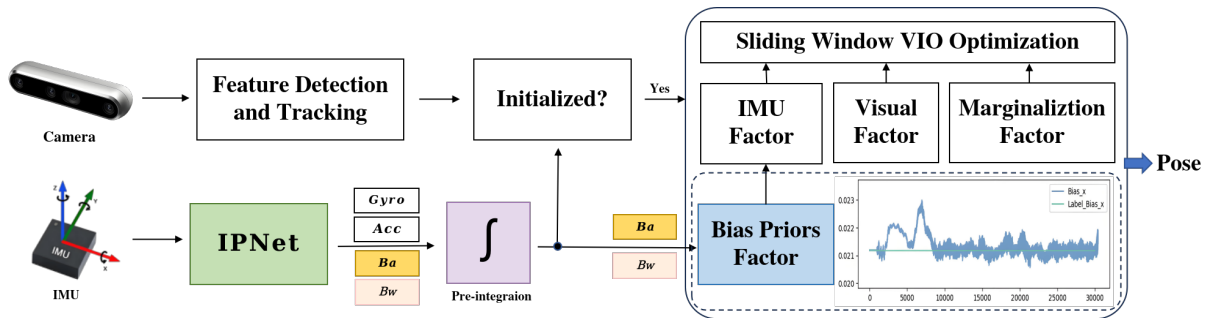


Fig. 2. The overview of the entire framework. Given image and IMU data, the framework outputs real-time pose information. At first, the IMU data is passed through the IPNet to estimate the current bias prior. Subsequently, the data stream is divided into two parts: one part inputs the bias prior along with the raw measurements into the pre-integration module, and performs optimization in the backend using IMU factors; the other part incorporates it as a prior factor into the factor graph, imposing reasonable constraints on the bias optimization process to ensure the precision of the bias estimation.

inertial datasets lack the ground truth bias, we introduce an iterative method to compute the average bias, which is then used for network training and experimentation. Overall, our main contributions are as follows:

(i) We propose IPNet, a novel network for real-time IMU bias estimation from raw data, eliminating recursive prediction dependency and preventing error propagation. By constructing bias estimates as a plug-and-play prior factor integrated into the VIO framework, the approach significantly enhances localization precision and robustness.

(ii) We introduce an iterative method to compute mean IMU bias, addressing the lack of ground truth in public datasets and providing reliable training labels.

(iii) Extensive experiments on public and self-collected datasets demonstrate significant improvements in localization precision and robustness.

II. RELATED WORK

A. Visual Inertial Odometry

The VIO algorithm was initially developed using the Extended Kalman Filter (EKF), primarily due to the computational limitations of early systems. This line of research has continued to evolve, with notable contributions including MSCKF [7], ROVIO [8], MSCKF 2.0 [9], OpenVINS [10], and SchurVINS [11]. With advancements in nonlinear optimization theory and improvements in computational power, optimization-based VIO methods have become the dominant approach. These methods integrate observational data and system constraints by formulating optimization problems, effectively overcoming the limitations of traditional filtering methods in handling complex nonlinear systems. Notable examples include OKVIS [12], VINS-Mono [4], ORB-SLAM3 [13], BASALT [14], Kimera [15], and DM-VIO [16].

However, existing methods often struggle to perform reliably under extreme conditions, such as low-texture environments or fast motion. These challenging scenarios can significantly degrade the accuracy of state estimation or even lead to system failures. As a result, improving the robustness of VIO algorithms remains a critical challenge in the field.

B. Learning Based Inertial Odometry

Learning-based inertial odometry has gained significant attention in recent years by combining traditional kinematic models with data-driven deep learning methods. One of the pioneering works, IONet [17], introduced a deep network-based inertial navigation system that predicts the displacement between adjacent IMU measurements, thereby mitigating error accumulation and generating relatively accurate trajectories. Building on similar tasks, Herath et al. [18] proposed a novel neural network architecture that achieves higher localization precision, particularly in challenging motion scenarios. Further advancing this line of research, Liu et al. [19] introduced TLIO, which leverages a neural network for 3D displacement estimation and integrates it with the EKF to produce high-fidelity trajectories. Subsequently, Sun et al. [20] proposed IDOL, a two-stage data-driven pipeline that first estimates orientation and then position, yielding improved localization results. Similarly, Zhang et al. [21] utilized deep neural networks to compute observable IMU integration terms, enhancing the precision and robustness of inertial navigation through numerical pose integration and sensor fusion.

In addition to trajectory estimation, many learning-based methods focus on IMU noise reduction and uncertainty estimation. For example, Brossard et al. [22] employed Convolutional Neural Networks (CNN) for gyro denoising. Steinbrener et al. [23] compared different architectures for denoising IMU measurements and found that Long Short-Term Memory Networks (LSTM) outperform Transformer architectures, especially under varying data rates. AirIMU [24] introduced an encoder-decoder network structure to process raw IMU data, estimating IMU states and uncertainties, and outputting corrected acceleration and angular velocity values along with their associated uncertainties. Zeinali et al. [25] proposed MobileResNet, a CNN-based lightweight block that utilizes deep and pointwise convolutions to reduce computational costs and noise interference, thereby improving navigation and localization. Moreover, Guo et al. [26] developed a dead reckoning algorithm for wheeled mobile robots by combining an Invariant Extended Kalman Filter with an IMU error model, enhanced by deep learning

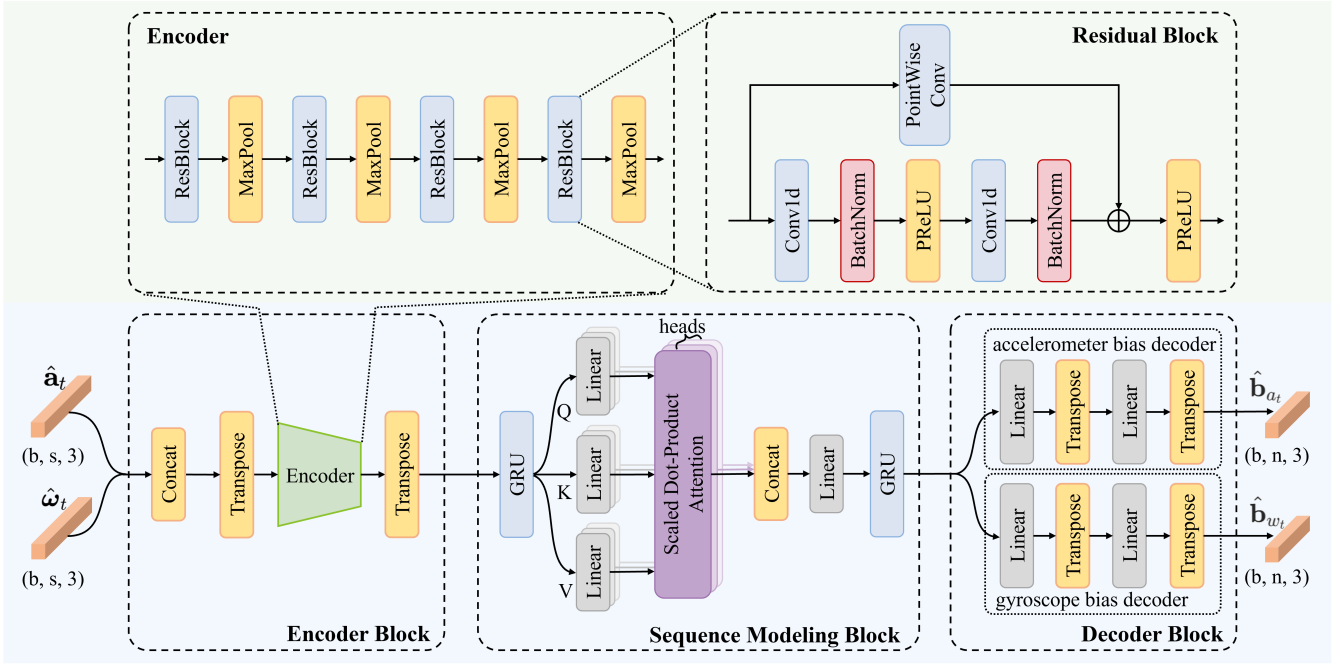


Fig. 3. The architecture of IPNet consists of encoder block, sequence modeling block and decoder block. The encoder block is mainly composed of four residual blocks and max-pooling layers, used to extract features and reduce the data dimension. The sequence modeling block is designed to further capture temporal dependencies and the decoder block is responsible for performing regression to predict the bias of both acceleration and angular velocity.

to estimate noise parameters. Yang et al. [27] integrated the Left-Invariant Extended Kalman Filter with a statistical neural network, proposing a learning-based dead reckoning algorithm that relies solely on inertial measurements and exhibits robust performance under sudden changes in lighting conditions.

However, existing methods still face challenges due to integration drift caused by accumulated noise and bias, which reduces the long-term accuracy of trajectory estimation. To address this issue, researchers combine IMU data with visual sensors and leverage deep learning to further improve both accuracy and robustness.

C. Learning Based Visual Inertial Odometry

Most of the current research on learning-based VIO focuses on the visual component, addressing various challenges faced by vision, such as blurred fields of view, sparse feature points, and so on. A smaller subset of studies focuses on utilizing learning-based methods to extract the potential information from IMU data for VIO. Danpeng Chen et al. [28] proposed a fusion of LSTM and a tightly coupled EKF framework to leverage IMU measurements, improving the robustness and precision of position estimation in visually constrained scenarios. Russell Buchanan et al. [6] introduced the first method to infer the evolution of bias using neural networks and integrated it as unary factors into a state estimator based on factor graphs. Subsequently, Solodar et al. [29] proposed VIO-DualProNet, which dynamically estimates the noise uncertainty of IMU data in real-time and fuses it into VINS-Mono [4] to enhance the robustness and precision of the system.

Unlike existing approaches, we revisit the network model for IMU bias prediction and propose a deep network that directly regresses the mean bias from raw IMU measurements, as detailed in Section III-B. Furthermore, we further developed an IMU prior factor based on this network, which can be easily integrated into any VIO method.

III. METHODOLOGY

The overview of our proposed framework is shown in Fig. 2. We use VINS-Fusion [5] as the baseline and integrate the plug-and-play learning-based IMU bias factor into it. This integration addresses a key challenge in VIO frameworks: the degradation of localization precision and robustness caused by inaccurate bias estimation due to visual tracking errors. Furthermore, to facilitate the acquisition of IMU bias labels for network training, we introduce a method for iteratively solving the bias using the ground truth pose and the ground truth velocity.

A. Preliminary

1) *IMU Noise Model*: Take \mathbf{a}_t and $\boldsymbol{\omega}_t$ as the true values of the IMU, and $\hat{\mathbf{a}}_t$ and $\hat{\boldsymbol{\omega}}_t$ as the measured values, both expressed in the body coordinate system. Considering the effects of bias, Gaussian white noise, and the gravitational acceleration in the world coordinate system, the IMU noise model can be expressed as:

$$\begin{aligned}\hat{\mathbf{a}}_t &= \mathbf{a}_t + \mathbf{b}_{a_t} + \mathbf{R}_w^t \mathbf{g}^w + \mathbf{n}_a, \\ \hat{\boldsymbol{\omega}}_t &= \boldsymbol{\omega}_t + \mathbf{b}_{w_t} + \mathbf{n}_w.\end{aligned}\quad (1)$$

where \mathbf{g}^w represents the gravitational force, \mathbf{R}_w^t stands for the rotation matrix between the world frame and the body frame,

\mathbf{b}_{a_t} and \mathbf{b}_{w_t} denote the accelerometer bias and gyroscope bias at time t , respectively, expressed in the body frame, and \mathbf{n}_a and \mathbf{n}_w describe the accelerometer noise and angular velocity noise.

2) *Preintegration*: We follow the discrete expressions in [30] and express the displacement, velocity, and rotational preintegration terms as $\alpha_{b_{k+1}}^{b_k}, \beta_{b_{k+1}}^{b_k}, \gamma_{b_{k+1}}^{b_k}$.

$$\begin{aligned}\alpha_{b_{k+1}}^{b_k} &= \iint_{t \in [t_k, t_{k+1}]} \mathbf{R}_t^{b_k} (\hat{\mathbf{a}}_t - \mathbf{b}_{a_t} - \mathbf{n}_a) dt^2, \\ \beta_{b_{k+1}}^{b_k} &= \int_{t \in [t_k, t_{k+1}]} \mathbf{R}_t^{b_k} (\hat{\mathbf{a}}_t - \mathbf{b}_{a_t} - \mathbf{n}_a) dt, \\ \gamma_{b_{k+1}}^{b_k} &= \int_{t \in [t_k, t_{k+1}]} \frac{1}{2} \Omega (\hat{\omega}_t - \mathbf{b}_{w_t} - \mathbf{n}_w) \gamma_t^{b_k} dt.\end{aligned}\quad (2)$$

where:

$$\Omega(\omega) = \begin{bmatrix} -[\omega]_{\times} & \omega \\ -\omega^T & 0 \end{bmatrix}, [\omega]_{\times} = \begin{bmatrix} 0 & -\omega_z & \omega_y \\ \omega_z & 0 & -\omega_x \\ -\omega_y & \omega_x & 0 \end{bmatrix}. \quad (3)$$

B. IPNet Model

We designed IPNet to directly predict the bias from raw IMU data. The network consists of three blocks: encoder block, sequence modeling block and decoder block, as shown in Fig.3. The raw IMU data represent the acceleration and angular velocity measurements in three dimensions, and we take a sample window of length s as the input to the model, so that the measurements can be denoted as $\hat{\mathbf{a}}_t \in \mathbb{R}^{s \times 3}$ and $\hat{\omega}_t \in \mathbb{R}^{s \times 3}$. We predict n values for each window to avoid prediction fluctuations. Therefore, the model outputs the predicted bias $\hat{\mathbf{b}}_a \in \mathbb{R}^{n \times 3}$ and $\hat{\mathbf{b}}_w \in \mathbb{R}^{n \times 3}$. In this paper, we set s to 1000 and n to 50.

1) *Encoder Block*: The encoder block mainly consists of several transformation layers to reshape the tensor and an encoder to capture local features and reduce data dimension. Firstly, concatenate $\hat{\mathbf{a}}_t$ and $\hat{\omega}_t$ along the last dimension, and then use the transpose operation to swap the positions of the last two dimensions, so as to facilitate the subsequent convolution operations. The encoder contains four sets of residual blocks and max-pooling layers. The main path of residual block primarily utilizes 1D convolution, batch normalization, and PReLU [31] activation, and the residual connection employs a pointwise convolution layer to combine the features of different channels and make the input and output have the same dimension, which are then added to the main path. Finally, a transpose operation is applied to restore the original dimensional order.

2) *Sequence Modeling Block*: The sequence modeling block is used to learn the temporal dependencies from the features output by the encoder, which consists of two Gated Recurrent Unit (GRU) layers with a multi-head self-attention [32] inserted between them. GRU is a kind of gated recurrent neural network. It controls the flow of information by introducing the update gate and the reset gate, thus realizing the modeling of long-term dependencies. The multi-head self-attention mechanism is used to further capture the relationships among different positions in the feature sequence, so that the model can focus on different context

information in different semantic subspaces through multiple linear transformations.

3) *Decoder Block*: To accommodate the characteristics of acceleration bias and angular velocity bias, the decoder block constructs separate accelerometer bias decoder and gyroscope bias decoder using linear layers and transpose operations to predict the bias for the three dimensions of acceleration and angular velocity, respectively. Additionally, to avoid instability caused by fluctuations in model predictions, each decoder outputs n predicted values, and their mean is used as the final prediction for each data window.

4) *Loss Function*: We use the Mean Absolute Error (MAE), to measure the difference between the predicted values and the ground truth. This loss pays more attention to the performance of the model on the majority of samples and is more robust to outliers. The final loss L is obtained by the sum of the L1 losses of the acceleration bias and the angular velocity bias. The formula is as follows:

$$L = L_{1_{b_a}} + L_{1_{b_w}} = \frac{1}{N} \sum_{t=1}^N |\mathbf{b}_{a_t} - \hat{\mathbf{b}}_{a_t}| + \frac{1}{N} \sum_{t=1}^N |\mathbf{b}_{w_t} - \hat{\mathbf{b}}_{w_t}|. \quad (4)$$

C. IMU Bias Prior Factor

The main purpose of this factor is to provide a relatively accurate initial value for the bias optimization. It evaluates the deviation between the actual bias value and the known initial value in the form of residual, and incorporates this constraint into the optimization problem, helping to reduce state drift. The definition of its residual is:

$$\mathbf{r} = \mathbf{W} \cdot \begin{bmatrix} \mathbf{r}_{b_a} \\ \mathbf{r}_{b_w} \end{bmatrix} = \mathbf{W} \cdot \begin{bmatrix} \mathbf{b}_{a_t, p} - \hat{\mathbf{b}}_{a_t} \\ \mathbf{b}_{w_t, p} - \hat{\mathbf{b}}_{w_t} \end{bmatrix}. \quad (5)$$

where $\mathbf{b}_{a_t, p}$ and $\mathbf{b}_{w_t, p}$ represent the final optimized results of the accelerometer bias and angular velocity bias at time t , respectively. The term \mathbf{W} represents the weight matrix, which controls the influence of the residuals on the optimization objective. Its Jacobian matrix is:

$$\mathbf{J}_r = \mathbf{W} \cdot \begin{bmatrix} \mathbf{I}_{3 \times 3} & \mathbf{0}_{3 \times 3} \\ \mathbf{0}_{3 \times 3} & \mathbf{I}_{3 \times 3} \end{bmatrix}. \quad (6)$$

D. IMU-Bias Label Solving Method

First, the raw IMU data is pre-integrated to obtain the measured values of the pre-integrated terms. These values are then subtracted from the ground truth of the pre-integrated terms to calculate the error. Finally, \mathbf{b}_{a_t} and \mathbf{b}_{w_t} are inversely solved through iterative calculations based on the first-order term of the pre-integrated with respect to bias changes. The formula is as follows:

$$\begin{aligned}\alpha_{b_{k+1}}^{b_k} - \hat{\alpha}_{b_{k+1}}^{b_k} &\approx J_{b_a}^{\alpha} \delta b_a + J_{b_w}^{\alpha} \delta b_w, \\ \beta_{b_{k+1}}^{b_k} - \hat{\beta}_{b_{k+1}}^{b_k} &\approx J_{b_a}^{\beta} \delta b_a + J_{b_w}^{\beta} \delta b_w, \\ \gamma_{b_{k+1}}^{b_k} - \hat{\gamma}_{b_{k+1}}^{b_k} &\approx \left[\frac{1}{2} J_{b_w}^{\gamma} \delta b_w \right].\end{aligned}\quad (7)$$

where the specific form of J refers to [4]. To directly obtain the mean values of \mathbf{b}_{a_t} and \mathbf{b}_{w_t} , similarity constraints can be further applied to iteratively derive the final IMU bias, which can be used as labels for network training.

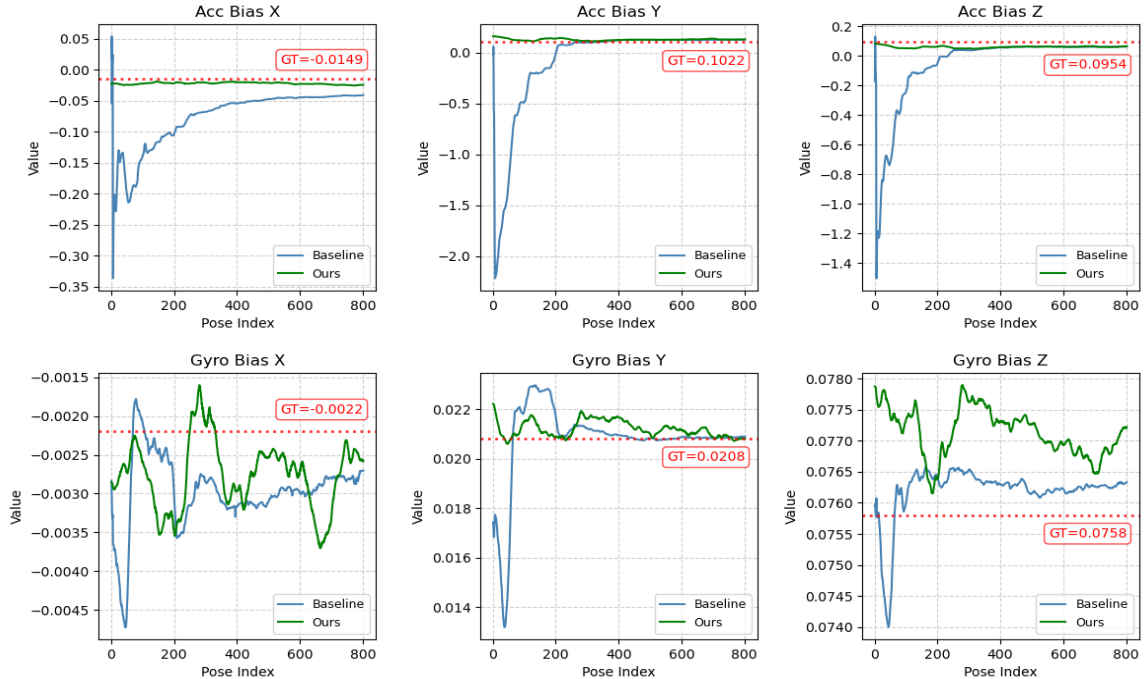


Fig. 4. The comparison of bias values curves corresponding to each pose in the V1.02 sequence. In the baseline, the bias values corresponding to the first 200 poses deviate significantly from the ground truth, whereas with our method, the bias values are quickly adjusted to fluctuate close to the ground truth. Blue: the bias predicted by baseline, Green: the bias predicted by our framework, Red: the ground truth bias.

IV. EXPERIMENTS

We conduct experiments on both public datasets and real-world scenarios to evaluate the proposed framework. In the first experiment, we select the combination of monocular vision and IMU from VINS-Fusion [5] as the baseline and conduct comparison studies to validate the localization precision and robustness on two public datasets. Furthermore, we test our framework on a self-collected dataset to assess its performance on low-cost IMU. Additionally, we use two public datasets with IMU bias labels to verify the accuracy of our iterative method.

A. Experimental Setup

1) *Datasets*: We select the EuRoC [33], TumVi [34], AR_Table [35] and in-house datasets for the evaluation. EuRoC: This dataset is widely used and consists of 20Hz drone images and 200Hz inertial data, with accurate the ground truth pose obtained through a motion capture system. Fortunately, each sub-dataset provides the ground truth of IMU bias, offering a valuable reference for verifying the effectiveness of our bias-solving method.

TumVi: This dataset was collected using handheld devices in various scenarios and is one of the commonly used datasets for evaluating VIO. It provides raw data sequences of two different image resolutions along with corresponding calibration sequences. It is worth noting that the IMU data in the calibration sequences have been corrected for bias. In our experiments, we compensate for this bias based on the parameters provided on the official website.

AR_Table: This dataset focuses on indoor tables as the collection target and aims to verify SLAM algorithms using planar features. Similar to the EuRoC dataset, it also provides accurate the ground truth pose and the ground truth bias through a motion capture system. Due to the dataset’s rich visual features, the IMU plays a limited role in constraints, so it is used solely to evaluate the accuracy of IMU bias computation.

In-house Dataset: To further validate the effectiveness of the framework, we select a low-cost IMU device, WHEEL-TEC N100, with a sampling frequency of 200Hz, and paired it with the Realsense D456 to form a simple visual-inertial data collection unit. The spatial position relationship of the hardware module is shown in Fig.5(c). We collected 12 data sequences in the environment shown in Fig.5(a), with a cumulative duration of about 20 minutes.

2) *Evaluation Metrics*: Firstly, to evaluate localization precision, we use Absolute Trajectory Error (ATE, m) and Relative Translational Error (RTE, m) as metrics, taking each sub-dataset as the smallest unit of evaluation, and select Root Mean Squared Error (RMSE) as the statistical basis. Secondly, to evaluate localization robustness, we describe it intuitively through the divergence and convergence of the trajectory. Finally, to evaluate the accuracy of the iterative method for calculating IMU bias, we compare the calculated results with the average values of each dimension in the sub-dataset individually.

3) *Implementation Details*: We implement the entire framework on a Lenovo Y9000P computer equipped with an

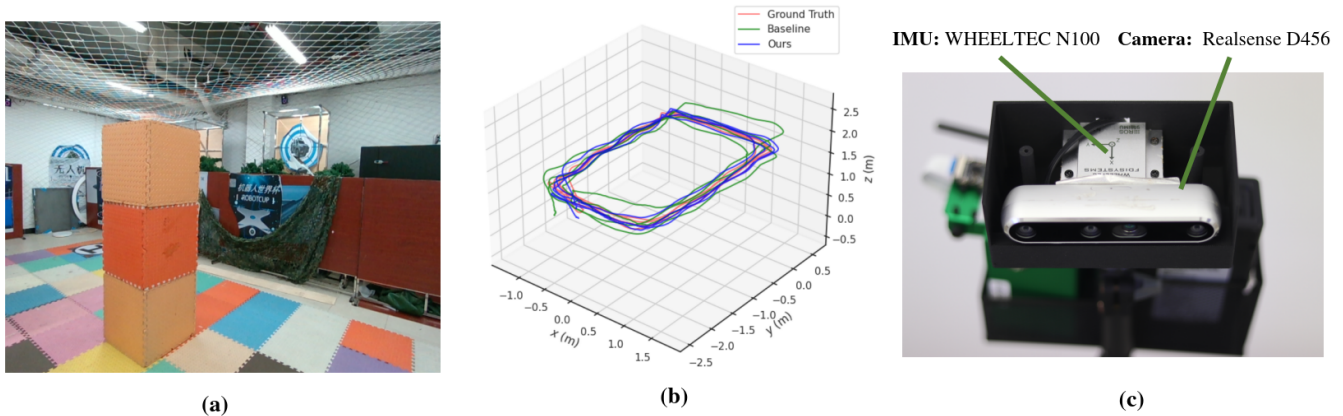


Fig. 5. (a) The image illustrates the specific environment and setup during the data collection process; (b) The image compares the differences between the trajectory generated by the baseline method and our proposed framework with the ground truth trajectory on the Seq02 sequence; (c) The image illustrates the spatial relationship between the IMU and the camera within our data acquisition system.

RTX 4090 GPU, running Ubuntu 20.04, and using OpenCV 3.4.5.

The proposed IPNet is designed and implemented using the PyTorch framework, with MAE as the loss function. The RMSprop optimizer is employed with an initial learning rate of $1e-6$, which is reduced by a factor of 10 after every 10 iterations. Other hyperparameter settings are provided in the source code. During the training of IPNet, we conduct a statistical analysis of the sample distribution in each sub-dataset and observe an imbalance in the data distribution. To address this, we adopt a strategy different from previous studies [6], [22], [24]. For the Euroc dataset, MH_01, MH_03, MH_04, V1_03, and V2_03 are used as the training set, MH_02 and V1_01 as the validation set, and the remaining data as the test set. For the TumVI dataset, room1, room2, and room4 are selected as the training set, room3 as the validation set, and the remaining two datasets as the test set. For the self-collected dataset, six sequences are chosen for the training set, two for the validation set, and the remaining four sequences for the test set.

We implement IMU bias estimation in PyTorch using a two-stage approach to obtain bias labels for network training. In the first stage, we calculate the bias of the gyroscope using the Adam optimizer with a learning rate of 0.001, 15000 iterations, and a 10-fold reduction in the learning rate every 5000 iterations. In the second stage, the gyroscope bias is fixed, and the bias of the accelerometer is calculated. The hyperparameters remain the same except for the learning rate, which is set to 0.01.

B. Performance

Tab. I shows a comparison of the performance between the baseline method and our framework on public datasets. The results demonstrate that our method achieves significant improvements, with the ATE-RMSE improving by an average of 46%, and the RTE-RMSE improving by an average of 8%. Additionally, the baseline method fails to track the trajectory of sequence V2.02 and room5, leading to divergence. This is primarily due to large visual

tracking errors in these sequences, combined with a low image processing frame rate of only 10Hz. The original inertial constraints are insufficient to compensate for the system, thus causing trajectory divergence. Taking the room5 sequence as an example, frequent shaking leads to drastic changes in the viewpoint, coupled with the limitation on the minimum distance for visual matching, which results in a limited number of feature points that can be correctly used at certain moments, ultimately causing the estimate to diverge. In contrast, our method introduces IMU bias prior, providing relatively accurate IMU constraints to the system, significantly improving the localization precision and robustness, even in situations with large visual errors.

TABLE I
ATE [M] & RTE [M]: PERFORMANCE ON PUBLIC DATASETS

Sequence	Baseline		Ours		
	ATE	RTE	ATE	RTE	
Euroc	MH_05	0.340	0.0074	0.249(27%)	0.0065(12%)
	V1_02	0.270	0.0101	0.106(61%)	0.0074(26%)
	V2_01	0.133	0.0138	0.048(64%)	0.0066(52%)
	V2_02	-	-	0.098*	0.0055*
TumVI	room5	-	-	0.436*	0.1044*
	room6	0.198	0.0352	0.102(48%)	0.0403(-15%)
Average		0.235	0.0166	0.126(46%)	0.0152(8%)

* Do not participate in the calculation of the average.

Fig.4 shows the variation of the bias corresponding to each pose during the VIO tracking process for the baseline and our methods in the V1_02 sequence. By introducing the prior, it is clearly observed that the bias are effectively constrained within a reasonable range. This approach not only improves the accuracy of bias estimation but also makes the optimization process more consistent with real physical constraints, thereby enhancing the overall stability and reliability of the optimization.

To facilitate a comparison with previous recursive prediction methods, we adopt the same training strategy for our

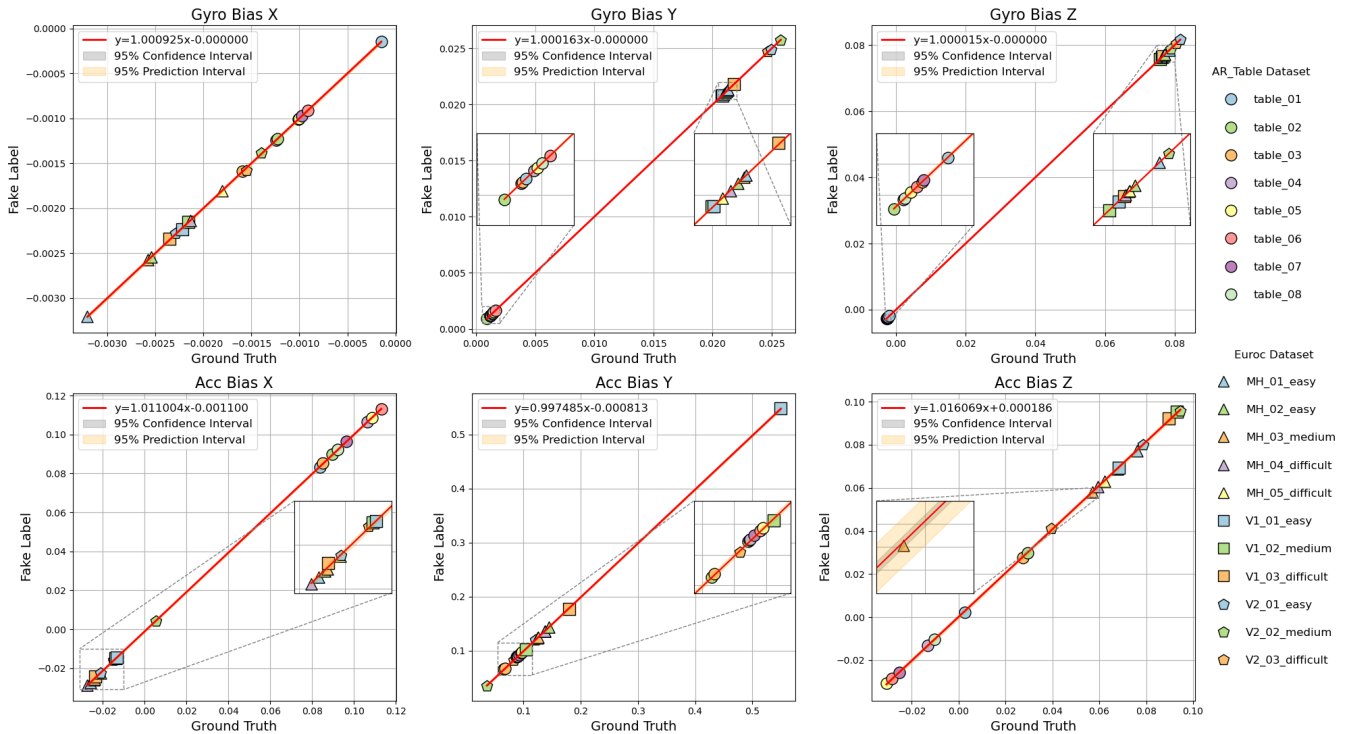


Fig. 6. IMU Bias Calculation Accuracy Experiment. The horizontal axis represents the ground truth bias, and the vertical axis represents the fake label of bias. Ideally, in the ideal case, they should be equal and distributed along a straight line with a slope of 1 and passing through the origin. The figure displays the bias distribution and fitting of different datasets. The gray area represents the confidence interval, used to characterize the 95% confidence interval of the fitting curve, while the yellow area represents the prediction interval, used to characterize the estimated range of future observation values under the 95% confidence level.

network and present the final localization results in Tab. II. The results show that our method outperforms the previous approaches.

TABLE II
ATE [M]: PERFORMANCE ON EUROc DATASET

Sequence	Zhang et al. [21]	Russell B. et al. [6]	Ours
MH_02	0.150	0.130	0.087
MH_04	0.138	0.250	0.188
V1_01	0.066	0.080	0.053
V1_03	0.147	0.170	0.147
V2_02	0.104	0.100	0.081

Tab. III shows the comparison results between our method and the baseline method on the self-collected dataset. Among them, Seq04 is purposely selected as a scene with high speed and drastic changes in the field of view. In this sequence, the original baseline on which the trajectories rapidly diverge, while our method can effectively maintain the tracking state and improve the robustness of the system. For the remaining sub-datasets, our method shows significant improvements in localization precision compared to the baseline, with the ATE-RMSE improving by an average of 46%, of which the trajectory comparison effect graph of the Seq02 sequence is shown in Fig.5(b). Due to the limitations in the number and layout of Vicon systems in the experimental environment, we deliberately reduce the rotation of the rigid body during

data collection to prevent frequent loss of ground truth data. As a result, no significant improvement is observed in the RTE-RMSE metric during testing. Overall, the experimental results are consistent with our findings on public datasets.

TABLE III
ATE [M] & RTE [M]: PERFORMANCE ON OUR DATASET

Sequence	Baseline		Ours	
	ATE	RTE	ATE	RTE
Seq01	0.2158	0.0490	0.1641(24%)	0.0494(-1%)
Seq02	0.2844	0.0436	0.0979(66%)	0.0430(1%)
Seq03	0.1390	0.0862	0.0806(42%)	0.0854(1%)
Seq04	-	-	0.5578*	0.0679*
Average	0.213	0.0596	0.1142(46%)	0.0593(0%)

* Do not participate in the calculation of the average.

C. IMU Bias Calculations VS. Labels

We validate the accuracy of our iterative method on the Euroc and AR_Table datasets and compare the calculated results with the ground truth average. The comparison results are shown in Fig.6. The slope and intercept of the curves in the figure clearly reflect the accuracy of the calculation, which can be directly used as labels for network training.

V. CONCLUSIONS

In this paper, we propose IPNet, which directly estimates IMU bias from raw data in real time and integrates bias

estimates as a plug-and-play prior factor into the VIO framework. The framework effectively reduces IMU bias estimation errors arising from unreliable visual features, thereby significantly improving localization accuracy and enhancing system robustness. The framework was implemented and evaluated across multiple datasets, with experimental results demonstrating that precise bias estimation leads to substantial improvements in overall system performance. In the near future, we aim to further optimize network training by incorporating noise labels for fine-tuning, ensuring that the estimations align more accurately and comprehensively with the IMU noise model.

REFERENCES

- [1] P. K. Panigrahi and S. K. Bisoy, "Localization strategies for autonomous mobile robots: A review," *Journal of King Saud University-Computer and Information Sciences*, vol. 34, no. 8, pp. 6019–6039, 2022.
- [2] J. Li, S. Yuan, M. Cao, T.-M. Nguyen, K. Cao, and L. Xie, "Hcto: Optimality-aware lidar inertial odometry with hybrid continuous time optimization for compact wearable mapping system," *ISPRS Journal of Photogrammetry and Remote Sensing*, vol. 211, pp. 228–243, 2024.
- [3] S. Dargan, S. Bansal, M. Kumar, A. Mittal, and K. Kumar, "Augmented reality: A comprehensive review," *Archives of Computational Methods in Engineering*, vol. 30, no. 2, pp. 1057–1080, 2023.
- [4] T. Qin, P. Li, and S. Shen, "Vins-mono: A robust and versatile monocular visual-inertial state estimator," *IEEE Transactions on Robotics*, vol. 34, no. 4, pp. 1004–1020, 2018.
- [5] T. Qin, S. Cao, J. Pan, and S. Shen, "A general optimization-based framework for global pose estimation with multiple sensors," *arXiv preprint arXiv:1901.03642*, 2019.
- [6] R. Buchanan, V. Agrawal, M. Camurri, F. Dellaert, and M. Fallon, "Deep imu bias inference for robust visual-inertial odometry with factor graphs," *IEEE Robotics and Automation Letters*, vol. 8, no. 1, pp. 41–48, 2023.
- [7] A. I. Mourikis and S. I. Roumeliotis, "A multi-state constraint kalman filter for vision-aided inertial navigation," in *Proceedings 2007 IEEE international conference on robotics and automation*. IEEE, 2007, pp. 3565–3572.
- [8] M. Bloesch, S. Omari, M. Hutter, and R. Siegwart, "Robust visual inertial odometry using a direct ekf-based approach," in *2015 IEEE/RSJ international conference on intelligent robots and systems (IROS)*. IEEE, 2015, pp. 298–304.
- [9] K. Sun, K. Mohta, B. Pfommer, M. Watterson, S. Liu, Y. Mulgaonkar, C. J. Taylor, and V. Kumar, "Robust stereo visual inertial odometry for fast autonomous flight," *IEEE Robotics and Automation Letters*, vol. 3, no. 2, pp. 965–972, 2018.
- [10] P. Geneva, K. Eickenhoff, W. Lee, Y. Yang, and G. Huang, "Opencvins: A research platform for visual-inertial estimation," in *2020 IEEE International Conference on Robotics and Automation (ICRA)*. IEEE, 2020, pp. 4666–4672.
- [11] Y. Fan, T. Zhao, and G. Wang, "Schurvins: Schur complement-based lightweight visual inertial navigation system," in *Proceedings of the IEEE/CVF Conference on Computer Vision and Pattern Recognition*, 2024, pp. 17964–17973.
- [12] S. Leutenegger, S. Lynen, M. Bosse, R. Siegwart, and P. Furgale, "Keyframe-based visual-inertial odometry using nonlinear optimization," *The International Journal of Robotics Research*, vol. 34, no. 3, pp. 314–334, 2015.
- [13] C. Campos, R. Elvira, J. J. G. Rodríguez, J. M. Montiel, and J. D. Tardós, "Orb-slam3: An accurate open-source library for visual, visual-inertial, and multimap slam," *IEEE Transactions on Robotics*, vol. 37, no. 6, pp. 1874–1890, 2021.
- [14] V. Usenko, N. Demmel, D. Schubert, J. Stueckler, and D. Cremers, "Visual-inertial mapping with non-linear factor recovery," *IEEE Robotics and Automation Letters (RA-L) & Int. Conference on Intelligent Robotics and Automation (ICRA)*, vol. 5, no. 2, pp. 422–429, 2020.
- [15] A. Rosinol, M. Abate, Y. Chang, and L. Carlone, "Kimera: an open-source library for real-time metric-semantic localization and mapping," in *IEEE Intl. Conf. on Robotics and Automation (ICRA)*, 2020.
- [16] L. Von Stumberg and D. Cremers, "Dm-vio: Delayed marginalization visual-inertial odometry," *IEEE Robotics and Automation Letters*, vol. 7, no. 2, pp. 1408–1415, 2022.
- [17] C. Chen, X. Lu, A. Markham, and N. Trigoni, "Ionet: Learning to cure the curse of drift in inertial odometry," in *Proceedings of the AAAI Conference on Artificial Intelligence*, vol. 32, no. 1, 2018.
- [18] S. Herath, H. Yan, and Y. Furukawa, "Ronin: Robust neural inertial navigation in the wild: Benchmark, evaluations, & new methods," in *2020 IEEE international conference on robotics and automation (ICRA)*. IEEE, 2020, pp. 3146–3152.
- [19] W. Liu, D. Caruso, E. Ilg, J. Dong, A. I. Mourikis, K. Daniilidis, V. Kumar, and J. Engel, "Tlio: Tight learned inertial odometry," *IEEE Robotics and Automation Letters*, vol. 5, no. 4, pp. 5653–5660, 2020.
- [20] S. Sun, D. Melamed, and K. Kitani, "Idol: Inertial deep orientation-estimation and localization," in *Proceedings of the AAAI Conference on Artificial Intelligence*, vol. 35, no. 7, 2021, pp. 6128–6137.
- [21] M. Zhang, M. Zhang, Y. Chen, and M. Li, "Imu data processing for inertial aided navigation: A recurrent neural network based approach," in *2021 IEEE International Conference on Robotics and Automation (ICRA)*. IEEE, 2021, pp. 3992–3998.
- [22] M. Brossard, S. Bonnabel, and A. Barrau, "Denoising imu gyroscopes with deep learning for open-loop attitude estimation," *IEEE Robotics and Automation Letters*, vol. 5, no. 3, pp. 4796–4803, 2020.
- [23] J. Steinbrener, C. Brommer, T. Jantos, A. Fornasier, and S. Weiss, "Improved state propagation through ai-based pre-processing and down-sampling of high-speed inertial data," in *2022 International Conference on Robotics and Automation (ICRA)*. IEEE, 2022, pp. 6084–6090.
- [24] Y. Qiu, C. Wang, C. Xu, Y. Chen, X. Zhou, Y. Xia, and S. Scherer, "Airimu: Learning uncertainty propagation for inertial odometry," *arXiv preprint arXiv:2310.04874*, 2023.
- [25] B. Zeinali, H. Zanddizari, and M. J. Chang, "Imunet: Efficient regression architecture for inertial imu navigation and positioning," *IEEE Transactions on Instrumentation and Measurement*, 2024.
- [26] F. Guo, H. Yang, X. Wu, H. Dong, Q. Wu, and Z. Li, "Model-based deep learning for low-cost imu dead reckoning of wheeled mobile robot," *IEEE Transactions on Industrial Electronics*, 2023.
- [27] D. Yang, H. Liu, X. Jin, J. Chen, C. Wang, X. Ding, and K. Xu, "Enhancing vio robustness under sudden lighting variation: A learning-based imu dead-reckoning for uav localization," *IEEE Robotics and Automation Letters*, 2024.
- [28] D. Chen, N. Wang, R. Xu, W. Xie, H. Bao, and G. Zhang, "Rninvio: Robust neural inertial navigation aided visual-inertial odometry in challenging scenes," in *2021 IEEE International Symposium on Mixed and Augmented Reality (ISMAR)*. IEEE, 2021, pp. 275–283.
- [29] D. Solodar and I. Klein, "Vio-dualpronet: Visual-inertial odometry with learning based process noise covariance," *Engineering Applications of Artificial Intelligence*, vol. 133, p. 108466, 2024.
- [30] C. Forster, L. Carlone, F. Dellaert, and D. Scaramuzza, "On-manifold preintegration for real-time visual-inertial odometry," *IEEE Transactions on Robotics*, vol. 33, no. 1, pp. 1–21, 2017.
- [31] K. He, X. Zhang, S. Ren, and J. Sun, "Delving deep into rectifiers: Surpassing human-level performance on imagenet classification," in *Proceedings of the IEEE International Conference on Computer Vision (ICCV)*, December 2015.
- [32] A. Vaswani, "Attention is all you need," *Advances in Neural Information Processing Systems*, 2017.
- [33] M. Burri, J. Nikolic, P. Gohl, T. Schneider, J. Rehder, S. Omari, M. W. Achtelik, and R. Siegwart, "The euroc micro aerial vehicle datasets," *The International Journal of Robotics Research*, vol. 35, no. 10, pp. 1157–1163, 2016.
- [34] D. Schubert, T. Goll, N. Demmel, V. Usenko, J. Stückler, and D. Cremers, "The tum vi benchmark for evaluating visual-inertial odometry," in *2018 IEEE/RSJ International Conference on Intelligent Robots and Systems (IROS)*. IEEE, 2018, pp. 1680–1687.
- [35] C. Chen, P. Geneva, Y. Peng, W. Lee, and G. Huang, "Monocular visual-inertial odometry with planar regularities," in *2023 IEEE International Conference on Robotics and Automation (ICRA)*. IEEE, 2023, pp. 6224–6231.